Determination of optimum camber distribution in rotating wings with deformable airfoils for vibration reduction and performance enhancement using surrogate modeling

Devesh Kumar, Bryan Glaz, Jiwon Mok, Peretz P Friedmann, Carlos E. S. Cesnik[†]

Department of Aerospace Engineering
The University of Michigan
Ann Arbor, MI 48109, U.S.A.

Abstract

This paper presents an optimization framework based on a low-order aeroelastic model of rotating wings with camber-wise deformable airfoils to enhance performance and vibration characteristics in rotorcraft. The baseline model is a scaled BO105 four bladed rotor used in the HART II experiments. The UM/NLABS-A code is used for 1-D beam analysis with camber actuation. The main section of each blade is divided into four segments along the span. The camber deformation amplitude and phase in each of the sections are considered design variables. In the first part of the study, frequency of the actuation is kept constant during the optimization process. However, different actuation frequencies were considered later to determine the most effective actuation frequency. Optimization has been conducted using the gradient-based optimizer *fmincon* in MATLAB, as well as a surrogate-based approach. Studies have been conducted to determine how the camber deflection profile along the blade span influences the rotorcraft performance and vibration at the hub. The optimized results are compared when the objective is modified to enhance the performance or to minimize the vibration.

Introduction

Reducing noise, vibration and power consumption are increasingly important for the modern helicopter industry. The current DARPA's Mission Adaptive Rotor program [1] aims to use morphing rotor technology to achieve following goals:

- 30% increase in useful payload fraction
- 40% increase in range performance
- 50% reduction in rotor acoustic detection range, at a minimum during the low-noise mission segments
- 90% reduction, due to active systems, of rotor-induced vibration – in all axes except about the rotor shaft (M_z) – for the low-vibration mission segments and no increase in vibrations over the baseline fixed-geometry rotor in other mission segments

Deformable airfoils present a unique way to contribute to vibration reduction and performance enhancement in rotating wings. Active twist rotors [2] can be seen as the first generation of morphing blades. Besides this, blades with active trailing edges have shown tremendous potential in reducing vibration, improving performance and reducing noise [3]. Camber deformation of the airfoil is seen as aerodynamically efficient alternative for controlling aerodynamic loads in order to obtain vibration reduction and performance enhancement. It has been shown that airfoil camber deformation can potentially be achieved by embedded smart actuators such as piezoelectric in the wing structure [4], or through compliant substructures such as airfoils with deformable leading edge ([5], [6]). Continuously deformable airfoils have already been considered for performance and handling-quality improvement of fixed-wing aircraft.

Kota and co-workers ([5], [7]) demonstrated the use of compliant mechanism for design of morphing aircraft structures. They suggested the use of passive compliant structures with a generic force actuator to produce static shape control of an airfoil camber. Gandhi and Anusonti-Inthra [8] looked at desirable attributes of a flexible skin on a morphing wing. Parametric study was conducted to determine the required in-plane and out-of-plane stiffness by considering requirement for actuation force, local and global deformation under aerodynamic loading and local buckling of skin. Santer and Pellegrino [6] introduced network analysis technique to determine an optimized compliant structure that deforms in conjunction with the wing skin in response to a single displacement actuation. Rediniotis et al. [9] demonstrated the use of shape memory alloys as artificial muscles to actuate a biomimetic hydrofoil. Kudva and co-workers ([4], [10]), as a part of the Defense Advanced Research Projects Agency (DARPA) sponsored Smart Wing program, developed deformable airfoil surfaces using ultrasonic piezoelectric motors and eccentuator to ensure effective transmission of motor torque to deflect control surface and demonstrated that the airfoil could achieve trailing-edge deflections of up to 20 deg at deflection rate of over 80 deg/s.

Use of conformable airfoils in rotorcraft blades has been limited. Anusonti-Inthra et al. [11] conducted research on conformable rotor airfoils using an optimized ground structure of piezoelectric elements. The predicted trailing-edge deflections were 4 deg, but the structure required a very large number of

[†] Corresponding author. 1320 Beal Avenue—3024 FXB, Ann Arbor, MI, 48109-2140, USA. E-mail: cesnik@umich.edu.

piezoelectric elements. Later, Gandhi et al. [12] proposed a conformable rotor airfoil design consisting of a passive compliant structure coupled with a limited number of piezoelectric actuators to reduce the complexity of the design.

In this paper, first, a global search over the parameter space – i.e., camber deformation amplitude, phase, and frequency of actuation – is conducted to identify the initial optimum points for the vibration and performance characteristics of the rotor blades with deformable airfoils. The optimization problem is solved using a surrogate-based approach in which the "true" objective functions and constraints are replaced with computationally efficient functional relationships. Since approximation errors can lead to sub-optimal solutions, an adaptive search methods based on the Efficient Global Optimization (EGO) algorithm, which accounts for uncertainty in surrogate predictions, is employed. Then starting from these optimum points of surrogated-based approach as initial points, gradient-based optimization is conducted using *fmincon* in MATLAB, to obtain the best results possible.

Optimization Framework

Overview

The mathematical optimization problem can be stated as:

$$min\ f(x) \tag{1}$$

subject to:

$$x_l \leq x \leq x_u \tag{2}$$

where f is the objective function, which can be the vibratory vertical hub load at 4/rev frequency (*F4Z*) or performance related moment (*M0Z*), x is the set of design variables that are bounded between a lower (x_l) and an upper (x_u) limits. As illustrated in Figure 1, the blade planform is subdivided in four regions of predetermined length. The design variables used in this optimization problem are the amplitudes and phases of the camber actuation at each of the four section for a given actuation frequency.

The optimization process involves two different steps shown in Figure 2. In the first step, initial range of design variables is given as input to create a surrogate model. Optimum results obtained from the surrogate model after multiple iterations are used as the initial values for the gradient-based optimization using MATLAB's *fmincon*. This process allows the gradient-based optimization to start from different initial feasible points and perform local search for minima.

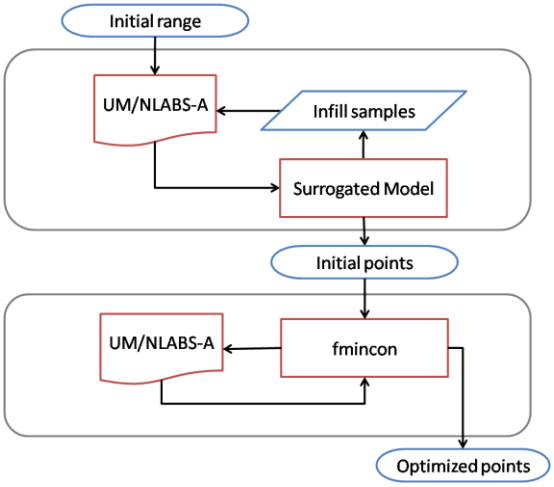

Figure 2: Two-step Optimization Process

Surrogate-based Optimization

The goal of using surrogate methods [13, 14] is to replace the true objective and constraints with smooth functional relationships of acceptable fidelity that can be evaluated quickly. In order to form the surrogate, the objective function must first be evaluated over an initial set of design points. The surrogate is then generated by interpolating the initial design points. Although function evaluations, which come from the expensive aeroelastic simulation, are needed to form the approximation, this initial investment of computer time is significantly less than that needed in a global search using non-surrogate based optimization methods. Once the surrogates have been created, they can be used to replace the more expensive "true" objective function in the search process for the global optimum. In this study, the vertical component of the 4/rev vibratory hub shear and performance metric are replaced by surrogates.

As discussed in Ref. [15], when the initial data set is produced by a deterministic computer code (as is the

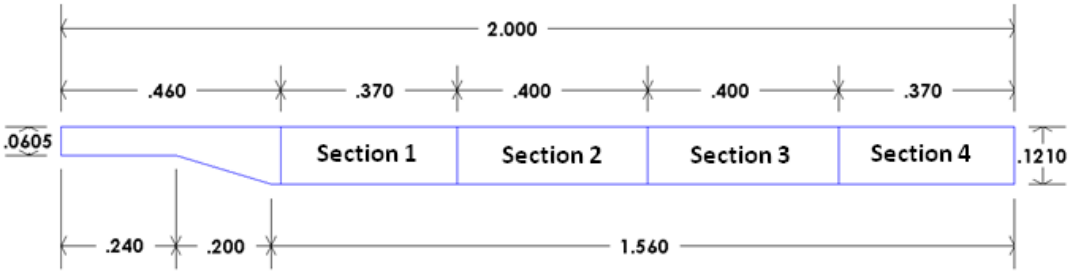

Figure 1: Blade Planform (All dimension in meters)

case here), "space-filling" designs of computer experiments should be considered. Detailed discussions of various space-filling designs can be found in Ref [14]. The MATLAB Latin hypercube function *lhsdesign* was used to generate the space-filling design of experiments used in this study. The points in the Latin hypercube represent design points at which helicopter simulations are to be conducted. Each simulation can be run independently of simulations at other design points; therefore the initial set of sample points is generated using distributed computers.

Once an initial set of fitting points have been produced, kriging interpolation [16, 17] is used to create the surrogate for the vibration and performance objective functions. Kriging interpolation is well suited to approximating nonlinear functions, and does not require a priori assumptions on the form of the function that is to be approximated. In kriging, the unknown function of interest, *y(x),* is assumed to be a random variable of the form

$$y(x) = g(x) + Z(x) \tag{3}$$

where *g(x)* is an assumed function (usually a low-order polynomial) and *Z(x)* is a stochastic (random) process. This is assumed to be Gaussian with zero mean and unknown variance that is estimated from the sample data. The regression model *g(x)* can be thought of as a globally valid trend function, while *Z(x)* accounts for local deviations from *g(x)*, ensuring that the kriging model interpolates the sample points exactly. The local deviations dictated by the sample points enable the kriging predictor to approximate nonlinear behavior regardless of the exact function's form. Note that although *y(x)* is deterministic rather than the stochastic process assumed in Eq. (3), kriging interpolation is still applicable. The assumption that *y(x)* is a random process is made because the deviation from the regression model can resemble a realization of a stochastic process [17]. Kriging has been used extensively for approximating nonlinear deterministic computer models [16]. The kriging surrogates were created with a freely available MATLAB toolbox [18].

Once the surrogate objective function is created using kriging, a potential method for finding the optimum is to optimize the surrogate directly, i.e., the "one-shot" approach. However if the surrogate is not accurate everywhere in the design space, the optimization may lead to local optima. Therefore, it is desirable to account for the uncertainty in the surrogate model since promising designs could lie in regions where the surrogate is inaccurate. The Efficient Global Optimization (EGO) algorithm [19] is an alternative to the "one-shot" approach which accounts for uncertainty in the surrogate and is more efficient. In EGO, a small number of initial design points are used to fit a kriging approximation. Based on the stochastic nature of kriging, an expected improvement function (EIF) is created in order to facilitate the selection of additional sample points (infill samples) where expensive computer simulations are to be conducted. These sample points are chosen to be where there is a high probability of producing a superior design over the current best design and/or where the predictions of the surrogate are unreliable due to a high amount of uncertainty. These infill samples represent a balance between the local consideration of finding an optimal design based on the information in the surrogate, and the global consideration of sampling in the design space where there is much uncertainty in the surrogate's predictions. Therefore, the EGO algorithm is able to adapt to potential errors in the approximate objective function by sampling at points at which there is much uncertainty in the surrogate's predictions. The kriging model is revised after the additional sample data is added to the initial data set, and the process of choosing additional sample points is repeated until a user defined criterion is satisfied. In summary, the advantages of such a method over the "one-shot" approach are: (1) a global search is conducted by sampling in regions with high uncertainty in the surrogate, and (2) fewer expensive function evaluations are required since a smaller initial sample set is used and additional sample points are selected in a more "intelligent" manner, as opposed to starting with a larger initial data set. The effectiveness of the EGO algorithm for passive design of helicopter rotors for vibration reduction was demonstrated in Ref. [20].

Gradient-based Optimization

A gradient-based constrained optimization is performed within MATLAB, using *fmincon* from its optimization toolbox. The *fmincon* function minimizes a constrained nonlinear multivariable problem. In each of the iteration, the function solves a quadratic programming subproblem. The gradients of the objective function and the constraints are provided from finite difference implemented in the framework. Since the objective function is highly nonlinear, and since the design hyperspace is very complex, it is possible for *fmincon* to fall into a local extrema, leading to a sub-optimal solution. Therefore, it is necessary to run the optimization to completion, starting from different initial points. These initial points are determined from the optimization done using the surrogate approach. When the problem is infeasible, *fmincon* attempts to reduce the distance to the most violated constraint boundary. Thus, it is recommended to start with a feasible initial point if possible. At the end of the cycle, the gradient-based optimization provides a better optimum than if only the surrogated was used.

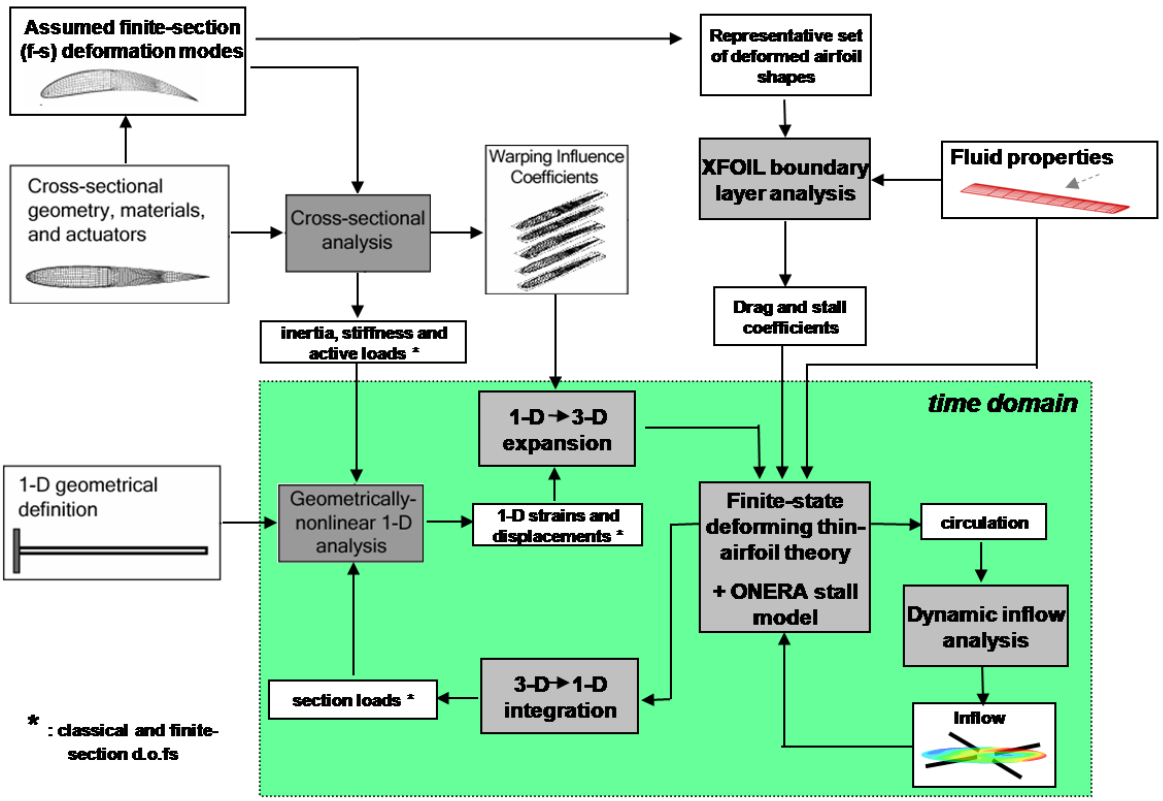

Figure 3: UM/NLABS-A Framework

Aeroelastic Framework (UM/NLABS-A)

In order to analyze morphing-type rotors, one must consider several effects normally assumed to be unimportant in rotor problems. A quasi-3D geometrically nonlinear model for the aeroelastic analysis of an airfoil with camber deformation was developed in UM/NLABS-A (Non-linear Anisotropic Beam Solver - Aeroelastic) [21, 22]. Schematic of the various components in the aeroelastic framework is shown in Figure 3 and details described next.

Structural model

The computational structural dynamics formulation used in the current study has been presented in Refs [23, 24]. It follows the variational-asymptotic method for the analysis of composite beams [25]; that is, the equations of motion for a slender anisotropic elastic three-dimensional solid are approximated by the recursive solution of a linear two-dimensional problem at each cross section and a one-dimensional geometrically-nonlinear problem along the reference line. This procedure allows the asymptotic approximation of the three-dimensional warping field in the beam cross sections, which are used with the one-dimensional beam solution to recover the three-dimensional displacement field. The present implementation adds an arbitrary expansion of the displacement field through a set of functions approximating the sectional deformation field to capture "non-classical" deformations, which are referred to as finite-section modes.

Aerodynamic Model

The low-order model uses the two-dimensional finite-state formulation for deformable airfoils presented in Ref. [26]. It is based on a Glauert expansion of the potential flow equations for a deformable airfoil of infinitesimal thickness. The camber-wise airfoil deformation is written using the Chebyshev polynomials of the first kind, which defines the generalized camber-wise displacement amplitudes. The wake-induced velocity is solved using the dynamic inflow theory. It assumes that the velocity normal to the rotor disk can be expressed in terms of radial and azimuthal expansion functions.

Drag and Dynamic Stall

A potential benefit of camber actuation is the ability to alter profile drag and stall characteristics, which have implications in power and vibration. To include these effects in the low-order model, the potential flow airload expressions are augmented with a quasi-static profile drag term as well as a dynamic-stall correction that is based on the ONERA model. The ONERA model assumes that the dynamic stall states are governed by a second-order differential equation, and requires static loading coefficients near and beyond stall. These are determined using the two-dimensional boundary layer analysis code XFOIL (which is valid to slightly post stall conditions),

along with a simple, empirically derived approximation for deep-stall. The coefficients are obtained under varying Reynolds number, angle-of-attack and camber deformation. A detailed account of the method used for determining the coefficients is available in Thepvongs et al. [21].

Coupling with Finite-State Aerodynamics

The finite-state aerodynamics formulation uses Chebyshev polynomials to form a basis for the camber deformations and associated airloads, while the choice of basis functions for the finite-section modes are arbitrary. The motion and force variables of the aerodynamics formulation are related to those of the structural formulation by a simple linear expression, as derived in Thepvongs et al. [21]. This straightforward connection between the aerodynamic and structural states allows the same space and time integration methods to be used for both formulations as well as a simultaneous solution. The governing structural dynamics equations, aerodynamic load expressions, dynamic stall equations and wake equations together define the time-domain problem. An explicit method is used with iterative refinement to achieve the desired convergence. A simple three-point backwards Euler time-integration scheme is used in accordance with the first-order form of the structural and potential flow governing equations. A four-point scheme is used to integrate the second-order dynamic stall equations.

Trim Analysis

The enforcement of vehicle equilibrium adds more variables and constraints to the aeroelastic problem. The present work assumes a wind-tunnel setup, where the variables are taken to be the collective, sine and cosine components of the cyclic pitch, and equilibrium is represented by specifying values for the time-averaged thrust, pitch and roll moments. These are provided by an autopilot that makes incremental changes to the control settings at every timestep. The "trimmability matrix" can be approximated by numerically computed Jacobian, determined by stepping the controls and examining the response at an instant one revolution later.

Camber Actuation

A parabolic camber centered at midchord was applied to the baseline airfoil shape. An example of an airfoil elastically deformed to modify the camber is shown in Figure 4. The 1% camber deformation shown in Figure 4 represents maximum deformation of 0.01c at the midchord. Murura et al. [27] also looked at combinations of plunge-camber and pitch-camber deformation besides the classical parabolic camber for aeroelastic analysis. Camber deformation in the current analysis is achieved by assigning an arbitrarily high cross-sectional stiffness and applying conjugate finite-section forces in the structural simulation. This method allows the user to control airfoil deformation without defining the particular actuation mechanism.

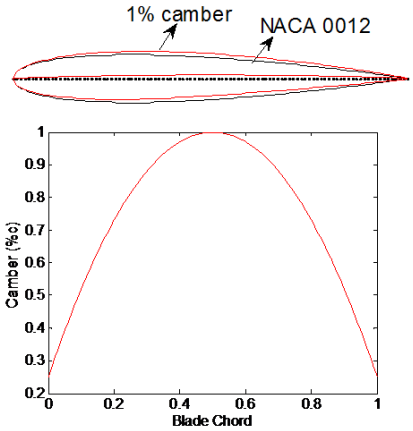

Figure 4: Airfoil Camber Distribution

Preliminary Investigation

Baseline Case

The baseline model is a scaled BO105 rotor with four blades, as used in the HART II experiments. Properties of the baseline rotor are summarized in Table 1 and more detailed information can be found in Ref. [21]. All cases consider here are at an advanced ratio of 0.25 and at a rotor thrust level of 3,100 N. Magnitudes of 4/rev hub vibration for all the load components for the baseline case are given in Table 2.

Table 1: Baseline blade properties

Property	Value
Type	Hingeless
Number of blades	4
Radius	2m
Root offset	0.44m
Chord	0.121m
Airfoil Section	NACA 0012
Operating RPM	109 rad/s
Advance Ratio	0.25
Shaft angle	-5 deg

Table 2: 4/rev vibratory hub loads for baseline case

Load Component	Value
$F4X_{base}$ (N)	40.15
$F4Y_{base}$ (N)	51.86
$F4Z_{base}$ (N)	15.58
$M4X_{base}$ (N m)	5.88
$M4Y_{base}$ (N m)	11.01
$M4Z_{base}$ (N m)	0.79

Circle Plots for F4Z vibration

Optimum range of design variables for optimization, with 4/rev vibratory vertical hub load as the objective function, were determined with the help of circle plots [28]. The "circle plots" present the sine and

cosine components of a vibratory response as function of the actuation phase for given actuation frequency and amplitude. For any given point in the plot, the amount of vibration is proportional to the distance to the origin of the graph. Circle plots were obtained for actuation frequencies from 2/rev to 7/rev and it was observed that 3/rev actuation frequency was the most effective in influencing 4/rev vibratory loads at the hub. The actuation forces on all four sections were assumed uniform. In this study, we considered twelve different camber actuation phase angles and three different camber actuation amplitude levels.

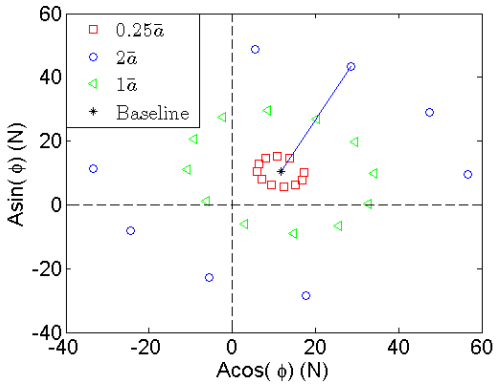

Figure 5: Circle plot for 4/rev vertical hub loads for 3/rev camber actuation (A and ϕ represent amplitude and phase, respectively, obtained from the FFT of the vertical hub load; the straight line from the baseline indicates zero actuation phase)

It can be seen from Figure 5 that curves coresponding to different amplitudes are almost centered around the baseline case and they enclose the origin. Camber deformtion in the current analysis is obtained by prescribing a distributed camber force along the span of the blade. Without loss of generality, uniform actuation force required to obtain camber deformation of 0.038% chord at the blade tip is referred to as $\bar{a}$, $2\bar{a}$ is twice this value, and 0.25 $\bar{a}$ is a quarter of it. Thus, the initial range for camber amplitude was chosen between no actuation and $2\bar{a}$. Corresponding camber deformation along the blade span for these cases is shown in Figure 6. Also, for simplicity, the camber stiffness of the blade was assumed to be constant along the blade span. In practical rotor blades, that is not the case and stiffness is higher closer to the root.

Phase of actuation was allowed to vary from 0 to 360 degrees. For these cases, the mean values of F_z (*F0Z*) was kept at its trim target of 3,100 N. Figure 7 shows that the maximum deviation from trim is less than 0.015%. Corresponding results shown in Figure 8 can be used to conclude that variation in mean M_z (*M0Z*) due to the camber actuation in this range is very small.

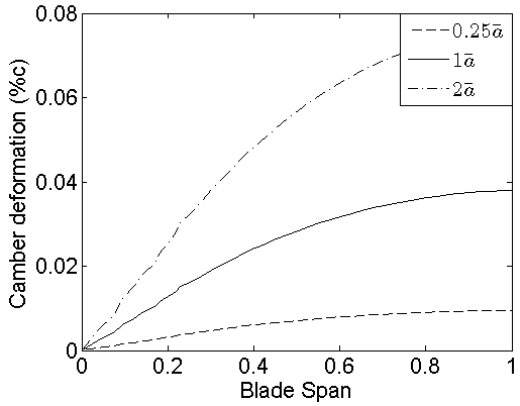

Figure 6: Camber deformation along the blade span

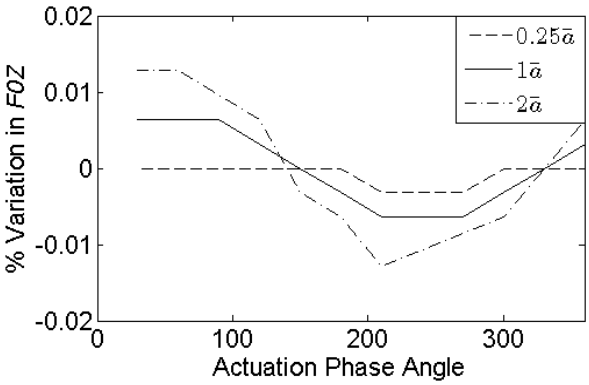

Figure 7: Percentage variation in vertical load at hub for 3/rev actuation frequency

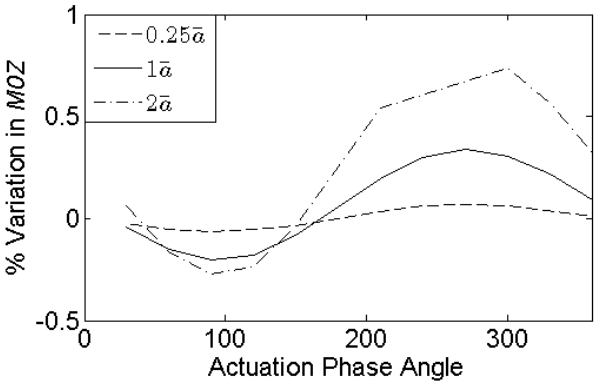

Figure 8: Percentage variation in hub torque for 3/rev actuation frequency

Optimization Results

Reduction of Vibratory Vertical Hub load

First, vertical hub load at 4/rev frequency (*F4Z*) was considered as the objective function. Actuation frequency was fixed at 3/rev based on the results obtained from the circle plots study described above. Results shown in Figure 9 indicate more than 95% vibration reduction at the end of the two-step optimization process. The bottom part of the column (in dark) represents the vibration reduction obtained just from the surrogate model optimization, while the top part (in gray) denotes additional improvement in

the result due to the gradient-based optimization. The maximum vibration reduction obtained was 99%. In order to overcome the presence of local minima, five optimized cases were considered. Amplitudes and phases corresponding to these cases are shown in Table 3 and 4, respectively. Initial values shown in Table 3 andTable 4 are the output of the surrogate optimization and input for the gradient-based optimization as described in Figure 2. The final values are optimized design variable values at the end of the novel two-step optimization process.

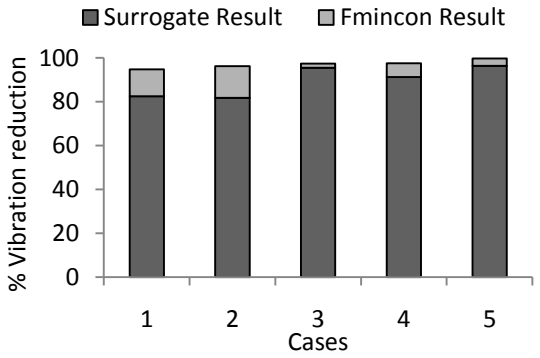

Figure 9: Percentage reduction is 4/rev vertical vibratory loads at the hub

Table 3: Normalized amplitude of actuation for optimized cases

Case		Amplitude of actuation ($\bar{a}$)			
		Sec 1	Sec 2	Sec 3	Sec 4
1	Initial	1.18	0.43	1.74	0.41
	Final	1.21	0.01	1.50	0.49
2	Initial	0.73	0.14	1.57	0.92
	Final	0.72	0.17	1.16	1.02
3	Initial	1.53	1.22	1.47	0.89
	Final	1.52	1.07	1.11	0.70
4	Initial	1.14	1.10	1.29	0.62
	Final	1.13	1.05	1.23	0.59
5	Initial	1.51	1.17	1.49	0.88
	Final	1.51	1.17	1.48	0.88

Table 4: Phase of camber actuation for optimized cases

Case		Phase of actuation (degrees)			
		Sec 1	Sec 2	Sec 3	Sec 4
1	Initial	140.4	217.1	150.1	165.6
	Final	148.2	206.9	161.5	165.7
2	Initial	107.1	260.7	164.4	150.7
	Final	109.7	255.6	177.9	155.4
3	Initial	218.0	240.0	113.8	141.0
	Final	203.7	216.5	122.4	136.9
4	Initial	216.9	192.9	132.5	141.9
	Final	223.6	200.0	131.2	143.7
5	Initial	219.4	238.5	114.5	144.0
	Final	218.6	236.9	116.4	145.7

To determine which section is most effective in reducing *F4Z*, a sensitivity study was conducted in Case 5 by perturbing the objective function around the optimum solution for each of the four blade sections separately. The actuation frequency is fixed to 3/rev. Results are shown in Table 5. As one can see, the sensitivity of the 4/rev vertical hub load to the camber actuation increases towards the outboard regions of the blade.

Table 5: Sensitivity analysis for 4/rev vertical hub load

Frequency	Sec1	Sec 2	Sec 3	Sec 4
Sensitivity (N/$\bar{a}$)	2.77	4.93	6.36	7.14

Figure 10 shows the variation in all the 4/rev vibratory hub load components for the Cases 4 and 5—the ones that indicated largest reduction in *F4Z*. As one can see, all the other load components are subjected to some reduction as well, with the exception of *M4X*. This can be addressed by bringing *M4X* to the objective function along with *F4Z*.

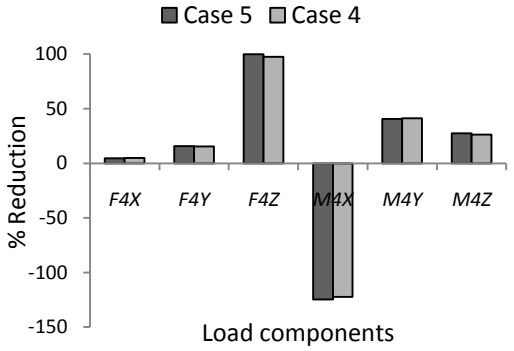

Figure 10: Variation in all 4/rev load components for the optimized Cases 4 and 5

Combined objective function for vibration reduction

To address multiple load components, the objective function is modified to include all the vibratory forces and moments at 4/rev frequency as

$$f(x) = \sqrt{(F4X)^2 + (F4Y)^2 + (F4Z)^2} + \frac{1}{R}\sqrt{(M4X)^2 + (M4Y)^2 + (M4Z)^2} \quad (4)$$

where R is the blade radius.

For the numerical study, four different frequencies of actuation were considered: 2/rev, 3/rev, 4/rev and 5/rev. Amplitude and phase of camber actuation force were the same for all the four sections of the blade—that is, the design variables among blade sections were linked together. Finally, the range for amplitudes considered was from zero to 15 $\bar{a}$. Results shown in Figure 11 indicate at least 46.5% reduction in combined vibratory hub loads due to camber actuation for different cases. The maximum of 50.2% vibration reduction was obtained in Case 4.

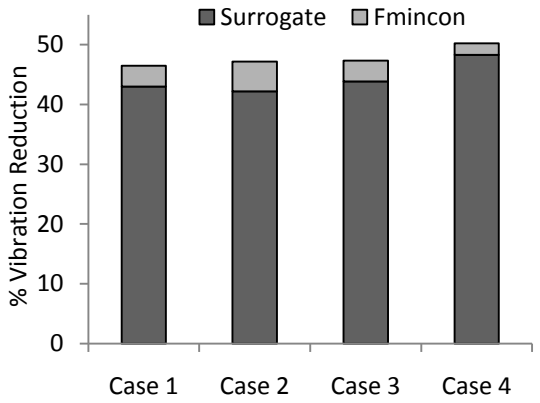

Figure 11: Percentage reduction in combined 4/rev vibratory load at the hub

Initial and final values of the design variables for the second phase of the optimization (*fmincon*) are shown in Table 6 and
Table 7.

Table 6: Amplitude of actuation for minimization of combined 4/rev vibratory loads at the hub

Case		Amplitude of actuation ($\bar{a}$) 2/rev	3/rev	4/rev	5/rev
1	Initial	14.48	0.87	0.07	5.94
	Final	14.79	1.06	0.03	5.73
2	Initial	14.82	0.93	0.05	2.86
	Final	15.00	1.11	0.00	2.53
3	Initial	14.39	0.88	0.20	6.38
	Final	15.00	1.09	0.00	6.62
4	Initial	14.60	0.96	0.09	14.23
	Final	14.61	1.27	0.09	14.24

Table 7: Phase of actuation for minimization of combined 4/rev vibratory loads at hub

Case		Phase of actuation (degree) 2/rev	3/rev	4/rev	5/rev
1	Initial	5.1	216.8	1.0	49.5
	Final	1.8	220.7	0.4	219.1
2	Initial	4.4	204.1	80.2	21.4
	Final	0.0	216.0	87.6	72.1
3	Initial	6.6	209.9	4.4	269.6
	Final	0.0	215.0	0.0	248.8
4	Initial	19.0	218.1	4.9	112.5
	Final	18.2	220.2	4.7	114.2

To determine which actuation frequency is most effective in reducing 4/rev combined vibratory hub loads, a sensitivity study was conducted for Case 4 by perturbing the optimum amplitude at each camber actuation frequency. Note that phase angles were not modified in this analysis. Results are summarized in Table 8, showing that the 4/rev vibratory hub load is most sensitive to 3/rev camber actuation in the rotating system. Therefore, the 3/rev camber actuation will provide the highest reduction in combined 4/rev vibratory hub loads.

Table 8: Sensitivity analysis for combined 4/rev vibratory loads

Frequency	2/rev	3/rev	4/rev	5/rev
Sensitivity (N/$\bar{a}$)	0.55	5.40	1.90	0.42

Variations in amplitude of 4/rev vibration for all the six components are shown separately in Figure 12 for Case 3 and Case 4. Maximum vibration reduction is obtained for *F4X* and *F4Y* component and they dominate the combined vibratory load as observed from results in Table 2.

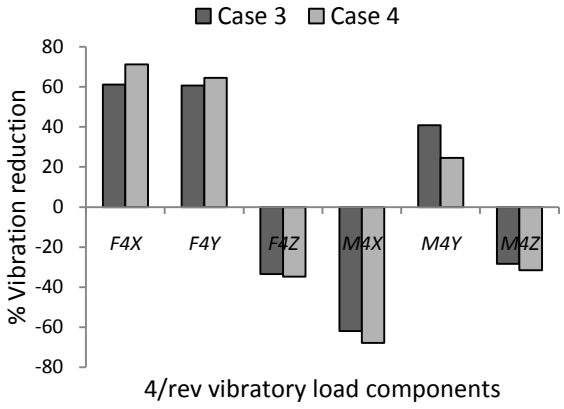

Figure 12: Variation in all 4/rev vibratory hub load components for the optimized cases

Optimization for performance enhancement
If the target is improving rotor performance, the mean value of the torque at the rotor hub (*M0Z*) can be used as the objective function for minimization. The range for amplitude was modified from no actuation to $4\,\bar{a}$ while the range for actuation phase was retained. As in the case for combined vibration reduction, four different actuation frequencies were considered: 2/rev, 3/rev, 4/rev and 5/rev. Amplitude and phase of actuation for a particular frequency are assumed to be same for all the sections of the blade.

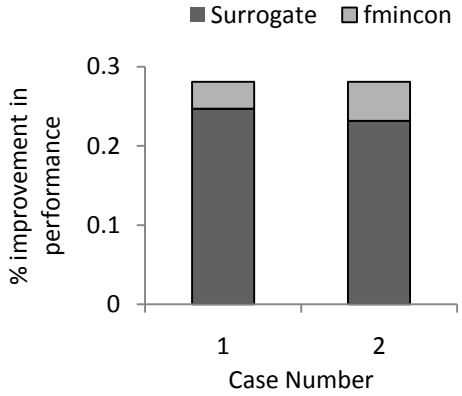

Figure 13: Percentage improvement in performance due to camber deformation

In the current operating conditions, the maximum performance enhancement that could be obtained was 0.28%. Initial and final values of the design variables for the optimized *fmincon* cases are given in Table 9 andTable 10. From the results shown, it is observed that 3/rev actuation frequency is the most effective in improving performance. The small effect on performance is due to the relatively low advance ratio chosen for this example (μ = 0.25). At this flight condition, no stall is present and, therefore, no stall correction is induced by camber adjustments on the retreating side. More studies are required at higher advance ratios to fully identify the potential of camber deformation for improving rotor performance.

Table 9: Amplitude of actuation for the optimized cases for performance enhancement

Case		Amplitude of actuation ($\bar{a}$) 2/rev	3/rev	4/rev	5/rev
1	Initial	0.05	2.34	0.05	0.91
	Final	0.02	2.03	0.00	0.00
2	Initial	2.64	1.94	0.06	0.71
	Final	0.00	2.06	0.00	0.00

Table 10: Phase of actuation for optimized cases for performance enhancement

Case		Phase of actuation (degrees) 2/rev	3/rev	4/rev	5/rev
1	Initial	2.2	98.6	4.7	338.4
	Final	2.2	96.0	4.7	338.4
2	Initial	277.8	97.2	68.0	144.5
	Final	303.5	95.8	85.4	144.5

As expected, optimizing for performance leads to increase in 4/rev vibratory loads at the hub. Figure 14 shows the increase in 4/rev hub vibration.

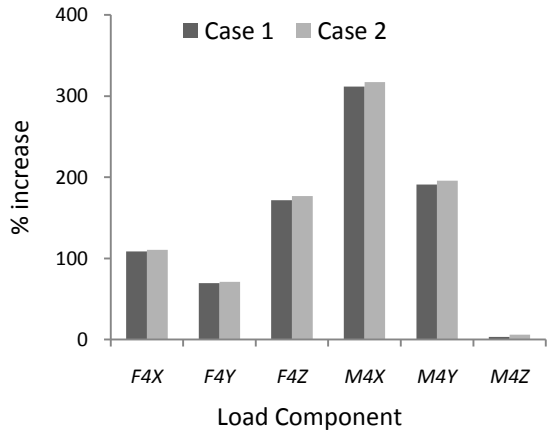

Figure 14: Percentage increase in 4/rev hub vibratory loads due to camber deformation for improvement in performance

Conclusions

This paper presents a novel two-step optimization process for determining optimum camber actuation in a morphing blade. The goal was to obtain reduction in vibratory loads and hub torque (as a metric of rotor performance). In the first step of the process, global search is performed using surrogated modeling to provide a good feasible initial design for the second step in the process: gradient-based optimization. The use of the gradient-based optimization allows one to improve convergence to a minimum, from the initial designs provided by the surrogated approach. Thus, a more stable optimization process is achieved, thereby reducing the overall required computational time. Final results obtained at the end of the gradient-based optimization showed additional improvement over the surrogate optimization results up to ~15%.

Exploratory studies of camber deformation for different frequencies, amplitude, and phases of actuation helped in selecting the range for the design variables needed for in the surrogate construction. The optimized results for the camber actuation showed it to be effective in:

- Reducing 4/rev vibratory vertical hub load (by more than 99%)
- Reducing combined 4/rev vibratory hub loads (by more than 50%)
- Improving the performance (by 0.28%)

In the current study, advance ratio of 0.25 has been considered. Camber actuation is expected to be more effective in improving performance and reducing vibration at higher advance ratios where dynamic stall effects become important.

References

[1] DARPA. "Mission Adaptive Rotor." http://www.darpa.mil/tto/programs/mar/ Aug, 2009.

[2] C. E. S. Cesnik, S-J. Shin, and M. L. Wilbur. "Dynamic Response of Active Twist Rotor Blades." *Smart Mat. and Struct.*, Vol. 10, 2001, pp. 62-76.

[3] L. Liu, P. P. Friedmann, I. Kim, and D. S. Bernstein. "Rotor Performance Enhancement and Vibration Reduction in Presence of Dynamic Stall Using Actively Controlled Flaps." *Journal of the American Helicopter Society*, Vol. 53, No. 4, May, 2006, 2008, pp. 338-350.

[4] J. N. Kudwa. "Overview of the DARPA Smart Wing Project." *Journal of Intelligent Material Systems and Structures*, Vol. 15, 2004, pp. 261-267.

[5] S. Kota, J. Hetrick, O. Russel, D. Paul, E. Pendleton, P. Flick, and C. Tilmann. "Design and Application of Compliant Mechanisms for Morphing

Aircraft Structures." *Proceedings of SPIE*, Vol. 5054, No. 24, 2003, pp. 24-33.

[6] M. J. Santer and S. Pellegrino. "Topology Optimization of Adaptive Compliant Aircraft Wing Leading Edge." *AIAA Structures, Structural Dynamics, and Materials Conference*, Honolulu, Hawaii, April, 2007.

[7] L. Saggere and S. Kota. "Static Shape Control of Smart Structures Using Compliant Mechnisms." *AIAA Journal*, Vol. 37, No. 5, 1999, pp. 572-578.

[8] F. Gandhi and P. Anusonti-Inthra. "Skin Design Studies for Variable Camber Morphing Airfoils." *Smart Materials and Struct.*, Vol. 17, 2008, pp. 1-8.

[9] O. K. Rendinotis, L. N. Wilson., D. C. Lagoudas, and M.M.Khan. "Development of a Shape-Memory-Alloy Actuated Biomimetic Hydrofoil." *Journal of Intelligent Material Systems and Structures*, Vol. 13, 2002, pp. 35-49.

[10] J. D. Bartley-Cho, D. P. Wang, C. A. Martin, J. N. Kudva, and M. N. West. "Developement of High-rate, Adaptive Trailing Edge Control Surface for the Smart Wing Phase 2 Wind Tunnel Model " *Journal of Intelligent Material Systems and Structures*, Vol. 15, 2004, pp. 279-291.

[11] P. Anusonti-Inthra, F. Gandhi, and M. Frecker. "Design of a Comformable Rotor Airfoil using Distributed Piezoelectric Actuation." Proceedings of *ASME International Mechanical Engineering Congress*, Washington, D.C., November 2003.

[12] F. Gandhi, M. Frecker, and A. Nissly. "Design Optimization of a Controllable Camber Rotor Airfoil." *AIAA J.*, Vol. 46, No. 1, 2008, pp. 142-153.

[13] A. Forester, A. Sobester and A. Keane. *Engineering Design via Surrogate Modelling*. A Practical Guide, AIAA, 2008.

[14] N. V. Queipo, R. T. Haftka, W. Shy, T. Goel, R. Vaidyanathan and P. K. Tucker. "Surrogate-based Analysis and Optimization." *Progress in Aerospace Sciences*, Vol. 41, 2005, pp. 1-28.

[15] T. W. Simpson, A. J. Booker, D. Ghosh, A. A. Guinta, P. N. Koch, and R. Yang. "Approximate Methods in Multidisciplinary Analysis and Optimization: A Panel Discussion." *Structural and Multidisciplinary Optimization*, Vol. 27, No. 5, 2004, pp. 302-313.

[16] J. Martin and T. Simpson. "Use of Kriging Models to Approximate Deterministic Computer Models." *AIAA J.*, Vol. 43, No. 4, 2005, pp. 853-863.

[17] J. Sacks, W. J. Welch, T. J. Mitchell, and H. P. Wynn. "Design and Analysis of Computer Experiments." *Statistical Science*, Vol. 4, No. 4, 1989, pp. 409-435.

[18] S. N. Lophaven, H. B. Nielsen, and J. Sondergaard. "A Matlab Kriging Toolbox, version 2.0." Informatics and Mathematical Modeling, 2002.

[19] D. R. Jones, M. Schonlau, and W. J. Welch. "Efficient Global Optimization of Epensive Black Box Functions." *Journal of Global Optimization*, Vol. 13, 1998, pp. 455-492.

[20] B. Glaz, P. P. Friedmann, and L. Liu. "Helicopter Vibration Reduction Throughout the Entire Envelope Using Surrogate-based Optimization." *Journal of American Helicopter Society*, Vol. 54, No. 1, Jan 2009.

[21] S. Thepvongs, C. E. S. Cesnik, R. Palacios, and D. A. Peters. "Finite-State Aeroelastic Modeling of Rotating WIngs with Deformable Airfoils." *American Helicopter Society 65th Annual Forum*, 2008.

[22] S. Thepvongs, J. R. Cook, C. E. S. Cesnik, and M. J. Smith. "Computational Aeroelasticity of Rotating Wings with Deformable Airfoils." Proceedings of *American Helicopter Soceity 65th Annual Forum*, Grapevine, Texas, May, 2009, 2009.

[23] R. Palacios and C. E. S. Cesnik. "Geometrically Nonlinear Theory of Composite Beams with Deformable Cross Sections." *AIAA Journal*, Vol. 46, No. 2, 2008, pp. 439-450.

[24] R. Palacios and C. E. S. Cesnik. "Low-Speed Aeroelastic Modeling of Very Flexible Slender Wings with Deformable Airfoils." *AIAA Structures, Structural Dyamics and Materials Conference*, Schaumburg, IL, April 2008.

[25] R. Palacios and C. E. S. Cesnik. "Cross-Sectional Analysis of Nonhomogenous Anisotropic Active Slender Structures." *AIAA Journal*, Vol. 43, No. 12, 5 July 2005, pp. 2624-2638.

[26] D. A. Peters, M. A. Hsieh, and A. Torrero. "A State Space Airloads Theory for Flexible Airfoils." *American Helicopter Society 63rd Annual Forum*, Phoenix, AZ, May, 2006.

[27] J. Murua, R. Palacios, and J. Peiro. "Camber Effects in the Dynamic Aeroelasticity of Compliant Airfoils." *International Forum on Aeroelasticity and Structural Dynamics*, Seattle, Washington, 2009.

[28] M. L. Wilbur, J. William T. Yeager, and M. K. Sekula. "Further examination of the vibratory loads reduction results from the NASA/ARMY/MIT active twist rotor." *American Helicopter Society 58th Annual Forum*, Montreal, Canada, June, 2002.